Article

Journal of
Nanoscience and Nanotechnology
Vol. 14, 4918–4929, 2014
www.aspbs.com/jnn

Tribological Properties of Polypropylene Composites with Carbon Nanotubes and Sepiolite

Victor H. Orozco[1,2], Andres F. Vargas[1,2], Witold Brostow[1,*], Tea Datashvili[1], Betty L. López[2], Kevin Mei[1], and Lisa Su[1,†]

[1] *Laboratory of Advanced Polymers and Optimized Materials (LAPOM), Department of Materials Science and Engineering and Center for Advanced Research and Technology (CART), University of North Texas, Denton, TX 76207, USA*
[2] *Grupo Ciencia de los Materiales, Universidad de Antioquia, Antioquía 050010, Calle 62 52 59 Medellín, Colombia*

Carbon nanotubes (CNTs) and sepiolite (SEP) were modified in order to improve their compatibility with the polypropylene (PP) matrix. Carboxylic groups were introduced into the CNTs through an oxidative treatment and aliphatic chains were incorporated on SEP by ion exchange of a cationic surfactant. Maleic anhydride grafted polypropylene (PPgMA) was mixed with neat PP to introduce polar groups into the polymer matrix. Composites including modified and non-modified fillers were prepared by melt extrusion. Dispersion and interaction of the CNTs with the PP and PPgMA matrices were evaluated by Raman spectroscopy while a focused ion beam/scanning electron microscopy (FIB/SEM) was used for SEP containing composites. Scratch resistance, microhardness, dynamic friction and wear were determined. Raman spectroscopy shows that the introduction of polar groups into PP matrices has a positive effect on the dispersion of modified CNTs. FIB/SEM results show that the modification of SEP improves its dispersion in the polypropylene matrix; filler clusters found in the PPgMA matrix are much times smaller than those in the neat PP. Despite of SEP agglomerates in the composites, a good interaction between both phases is seen; SEP particles are fully coated and embedded inside the PP matrix. The 'lack of cooperation' between unmodified PP and its fillers results in nanocomposites with larger residual depths; by contrast, PPgMA does 'cooperate' with its fillers so that the nanocomposites in scratch resistance testing have smaller residual depths R_h than the neat PPgMA. Addition of the fillers to PPgMA also increases the hardness. As for wear rates, some our fillers provide higher and some lower wear rates than PP.

Keywords: Polypropylene, Sepiolite, Carbon Nanotubes, Nanohybrids, Scratch Resistance, Wear, Dynamic Friction.

1. INTRODUCTION

Polymers and polymer-based materials (PBMs) have emerged as a predominant class of materials in a multitude of applications ranging from simple plastic bottles to great engineering achievements such as space shuttles and the Boeing 787 Dreamliner. Among PBMs, polypropylene (PP) remains an industrial favorite due to its low cost and accessibility as well as its high strength and high modulus.[1] PP has applications in a variety of industries, ranging from automobiles via textiles to medical technologies. However, PP suffers from low impact resistance and low service temperature range. One possible solution to compensate for these drawbacks is the use of additives or reinforcements[2] such as fibers or fillers. Properties of the resulting composites are influenced by the nature of the components, dispersion and the shape of the filler, the morphology of the system, and compatibility between the phases.[3–22] In particular, interfaces are important.[23–25] Thus a large variety of properties can be obtained solely by alteration of one of these factors.

Despite progress made, we need more experimental data to understand the influence of various fillers on composite properties. While significant effort has already been expended on mechanical properties, in all cases when polymeric parts are in motion *wear* is especially important. Rabinowicz[26] has argued convincingly about the

*Author to whom correspondence should be addressed.
†Present address: Now at Stanford University, Stanford, CA 94305, USA.

 1533-4880/2014/14/4918/012 doi:10.1166/jnn.2014.8289

importance of wear for economic well-being of industrial companies to prevent economic crises in entire countries.

In this situation we decided to investigate the effects of two types of nano fillers, namely carbon nanotubes (CNTs) and sepiolite (SEP) on tribological performance of PP and PP containing composites.

For development of PP + CNTs and/or PP + SEP nanohybrids with desirable properties, it is crucial to improve interfacial bonding. Namely, CNTs and sepiolite must overcome incompatibility and poor dispersion within the PP matrix. In order to address these issues we have used two different approaches. The first was functionalization of the fillers, a process by which the nanoparticles undergo surface modification to improve molecular interactions;[14] the second approach consists in blending bare and functionalized fillers with maleic anhydride modified PP, obtaining PPgMA.[20]

2. EXPERIMENTAL PART

2.1. Materials

Commercial grade PP and PPgMA (Epolene G-3003) with 0.8 wt.% of maleic acid (MA) were received from Dow Chemical (DOW h777-25R Polypropylene Resin) and Eastman, respectively. Multi-wall carbon nanotubes (CNTs) with 90 wt.% purity were obtained from Nanocyl. The CNTs were approximately 10 nm wide and 0.1–10 μm in length. Micronized sepiolite (SEP) was purchased from the Spanish company Tolsa while nitric acid and cethyl trymethyl ammonium bromide (CTABr) were received from Sigma-Aldrich.

All the chemicals were analytical grades and have been used as received.

2.2. Characterization Techniques

2.2.1. Dynamic Friction from a Pin-on-Disk Tribometer

Dynamic friction has been determined using a Nanovea pin-on-disk tribometer from Micro Photonics Inc. A pin applies a vertical force to a material surface, with that surface moving on a circular disk at a constant angular speed. The equipment provides also a capability to apply lubricants but this option was not used. Each test was conducted under 5.0 N, 10.0 N and 15.0 N of normal force, at 21 ± 2 °C, 1 atm. Stainless steel 302 (SS302) and tungsten carbide (WC) balls were 0.32 mm in diameter. Tungsten carbide is much harder than steel, hence different behavior of the surfaces investigated with respect to those two pins was expected. The disk spun at 100 rpm, to cover a distance of 3000 m in about 23 minutes for a total of 2300 revolutions. Friction and other tribological techniques applied to polymers have been reviewed before.[27–29]

2.2.2. Wear

We have calculated the wear rates associated with tracks obtained through tribometry testing. The wear rate W for each track is calculated as:

$$W = 2\pi rA/(Fd) \quad (1)$$

where r is the track radius, A is the track cross-sectional area, F is the load and d is the total distance covered in the tribometry test. The r.h.s. numerator represents the total volume displaced by the tribometer in the test.

2.2.3. Vickers' Microhardness

Microhardness tests were performed with a Shimadzu Microhardness Tester to determine the Vickers hardness number h_{Vickers}. Each sample was indented for 10 secconds under 3 different loads: 100 N, 300 N and 500 N. After measuring the diameter of the indentation, h_{Vickers} was calculated as

$$h_{\text{Vickers}} = 1854.4 \cdot P/d^2 \quad (2)$$

where P is the load and d is the mean diagonal of the indentation. The data reported represent the averages of five indentations each.

2.2.4. Thermogravimetric Analysis (TGA)

TGA equipment from a TA Instruments Q500 was used to study the thermal stability of the composites and the progress of CNTs oxidation process. The samples were heated from 25 to 800 °C at the heating rate of 10 °C/min. The technique has been well described by Lucas and her colleagues,[30] Menard,[31] and Gedde.[32]

2.2.5. Fourier Transform Infrared Spectroscopy (FTIR)

The FTIR spectra were recorded with a Perkin-Elmer Spectrum One spectrometer; powdered samples were dispersed in KBr and thin disks were prepared and analyzed in the transmission mode.

2.2.6. Raman Spectroscopy

An Almega XR Raman Spectrometer equipped with a 532 nm laser was used to obtain the Raman spectra of the samples within the 4000–100 cm^{-1} range. Collect exposure, preview exposure, and sample exposure times were respectively 10, 0.5 and 4 seconds.

2.2.7. Scratch Resistance

A Micro-Scratch Tester (MST) from CSM, Peseux, Switzerland was used. Each sample underwent linearly progressive scratch testing using the following parameters: initial load 5.0 N, final load 30.0 N, loading rate 10.0 N/min. The conical diamond indenter had a diameter of 200 μm and a cone angle of 120°. The scratch testing conditions were identical for all samples. This technique has been described before.[28, 29]

2.2.8. Focused Ion Beam/Scanning Electron Microscope (FIB/SEM)

We have used a technique described before.[20, 33, 34] The FEI Nova 200 NanoLab (a dual column ultra-high resolution

field emission scanning electron microscope (SEM) and focused ion beam (FIB)) were used to study the morphology of the composites. A small fraction of the samples were mounted on a copper stub and coated with a thin layer of gold and palladium to avoid electrostatic charging during examination.

2.3. Treatment of Filler Materials

We have used carboxylic groups and alkyl chains of CTABr to modify the surfaces of CNTs and sepiolite, respectively.

2.3.1. Oxidation of CNTs

CNTs were dispersed in nitric acid via ultrasonic bath in a weight ratio of 25:300 for 30 min at 80 °C. Afterwards, the CNTs were refluxed over 48 hours. At the end of the process the oxidized CNTs (CNTOs) were washed several times until neutral pH was obtained. The CNTOs were dried in a vacuum oven at 40 °C.

2.3.2. Functionalization of Sepiolite

1.1 g of CTABr was dissolved in 450 mL of water and continuously stirred at 35 °C. After 2 hours of mixing, 30 g of SEP were added into the solution and the mixing was maintained for one more hour. The slurry was left overnight, then it was centrifuged and the functionalized sepiolite (SEPF) was vacuum dried at 40 °C overnight.

2.4. Sample Preparation

Prior to processing the composites, we had manually mixed pelletized PP with pelletized PPgMA and with either powdered SEP, SEPF, CNTs or CNTOs. Using a co-rotating intermeshing twin screw extruder (Thermo Haake, diameter of the screw = 16 mm, length/diameter = L/D = 25) at 100 rpm, we melt-extruded the samples while maintaining temperature of the extruder at 110, 170, 200, 200 and 200 °C in the five zones from hopper to the die. Details have been described by Vargas and coworkers.[21] The sample compositions are listed in Table I.

Table I. The sample compositions.

Sample	PP (%)	PPgMA (%)	CNT (%)	Sepiolite (%)	CNTO (%)	Sepiolite func (%)
PP	100	0	0	0	0	0
PP + PPgMA	90	10	0	0	0	0
PP + CNT	99.25	0	0.75	0	0	0
PP + PPgMA + CNT	89.25	10	0.75	0	0	0
PP + SEP	99.25	0	0	0.75	0	0
PP + PPgMA + SEP	89.25	10	0	0.75	0	0
PPCNTO	99.25	0	0	0	0.75	0
PP + PPgMA + CNTO	89.25	10	0	0	0.75	0
PP + SEPF	99.25	0	0	0	0	0.75
PP + PPgMA + SEPF	89.25	10	0	0	0	0.75

3. MODIFICATION OF THE CNTs AND SEP

Thermogravimetric analysis (TGA) and Fourier-transform infrared (FTIR) techniques have been used to confirm functionalization. For CNTOs, we used TGA to observe increased water desorption due to formation of hydrophilic moieties. In Figure 1, CNTOs show strong decomposition at temperatures much below those at which CNTs decompose, due to oxidative scission and shortening of CNTs.[35, 36] Thus, oxidation of CNTs decreases thermal stability.

Interactions between the modifier and SEP surfaces were monitored by FTIR spectroscopy. Figure 2 shows FTIR spectra of the SEP before and after modification.

SEP is a hydrous magnesium silicate, namely $(Si_{12}Mg_8O_{30})(OH)_4(OH_2)_4 \cdot 8H_2O$.[37] In order to improve the dispersion of the particles within the hydrophobic polymer matrix, SEP was treated with a cationic surfactant (CTABr), which has the capability to exchange Mg^{+2} ions of the SEP by positively charged amine groups and at the same time introducing alkyl chains from cethyl group,[19] that can enhance the compatibility of SEP with PP.[38]

As we see in Figure 2, after the cationic exchange treatment two new peaks appeared at 2926 and 2853 cm^{-1}; they correspond to the C—H stretching—what confirms the successful ionic exchange of CTABr on SEP.

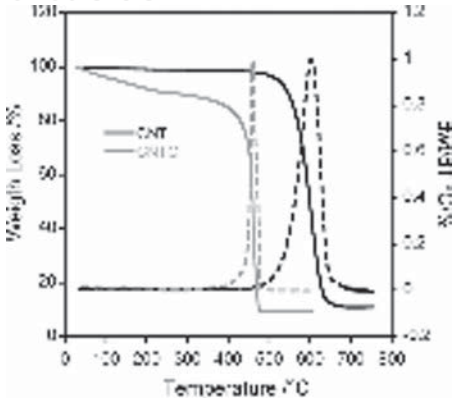

Figure 1. TGA of CNTs before (CNT) and after oxidation (CNO).

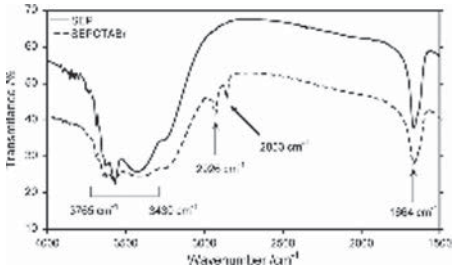

Figure 2. FTIR of sepiolite before and after modification.

4. FILLER DISPERSION ANALYSIS BY RAMAN SPECTROSCOPY AND FIB/SEM

Raman spectroscopy is a convenient tool for characterization of polymer + CNTs nanohybrids. We have used Raman spectroscopy with OMNIC μs mapping capability to identify the regions filled with CNTs and to analyze dispersion of the filler in the polymer matrix.

Figure 3 presents the Raman spectra of CNTs, PP, PPgMA and their composites. In contrast to neat PP and PPgMA, two new peaks were found for CNTs containing samples at the spectral range of 1200–1700 cm^{-1}. A Raman band around 1598 cm^{-1} is associated with the *G* band or tangential mode which corresponds to the C—C stretching mode in the graphitic plane. There is a very small band at 1300 cm^{-1} that is associated with the *D* band; it is the defect mode that reflects the presence of disordered graphite structures.

After modification of CNTs, the *G* band becomes smaller. Weakening and slight shifting of the band can be attributed to disentanglement of nanotubes and subsequent dispersion in the PP matrix—a consequence of better polymer penetration into the modified nanotubes bundles during the melt mixing process.

Distribution analysis of the CNTs inside PP and PPgMA was conducted via Raman mapping. We have also used an Olympus BX51 microscope to collect the surface images of the composites during Raman linear mapping; see Figure 4.

In contrast to PP + CNTs samples, we observed less particles agglomeration for PP and PPgMA composites with modified CNTs. From 50 μm scale surface image of PP + CNTs band, we see numerous black spots attributed to nanotube agglomerates in Figure 4(A). Microscopic evaluation of the composite surfaces shows improved CNTs dispersion after modification of CNTs and hydrophobic nature of PP. Overall, the best uniformity of particles dispersion is found for the sample based on modified filler and modified PP. Thus, the introduction of polar groups into PP matrix has a positive effect on dispersion of CNTs. Figure 5 presents Raman linear mapping spectra.

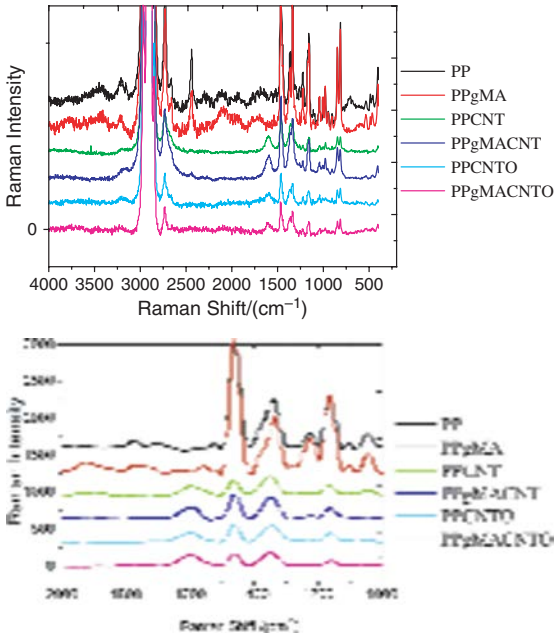

Figure 3. Raman spectra of PP and nanocomposites.

The intensity of the Raman band is shown in colors, with red representing the most intense CNTs bands and blue indicating virtually no spectral intensity for that Raman band. CNTs dispersion in PP and PPgMA phases were investigated using linear mapping data. One calculates a correlation between the sample map spectrum and a specific reference spectrum. In this case we have used the 'naked' CNTs spectrum as a reference. The composite with a higher intensity value indicates a greater similarity to the CNT as a reference spectrum. A correlation value of 1.0 (or a red color) indicates that the spectrum from that region of the map and the reference spectrum are nearly identical. Figure 5 shows that the CNTOs are better dispersed than non-oxidized ones, although CNTs shows also good dispersion in the presence of PPgMA.

Linear mapping displayed in Figure 6 was performed using a 532 nm laser with 10 s exposure time per 10 μm size step, with a total of 5 collection points.

From the 3D images of Raman spectra we can observe changes in intensity of the characteristic C—C stretching modes of the graphitic plane at approximately 1598 cm^{-1} spectrum range for a total of 5 collection points. We also see from Figure 6 that the Raman intensity peaks at ~1600 cm^{-1} are quite flat and level with a relatively small standard deviation of the normalized Raman intensity for the PPgMA + CNTs and PPgMA + CNTOs samples, indicating that the nanotubes are well distributed in the PPgMA matrix. In contrast, there are several big peaks in the Raman map of PP + CNTs, showing that in this material the nanotubes are poorly dispersed. From Raman linear mapping we find improved but still not quite uniform filler dispersion for unmodified PP samples filled with oxidized CNTs.

Let us return now to the composites filled with SEP particles. For these composites we used FIB/SEM to investigate the dispersion of the filler particles in the PP and PPgMA phases. SEM images of the composites at a length scale of 300 and 400 nm are presented in Figure 7.

Figure 7 shows that either SEP particles treatment or PP phase modification prevents particle agglomeration. Compared to the neat PP matrix, more particle agglomeration is seen for PPgMA samples. We infer from these micrographs that the polar groups of the polymer matrix do not promote uniform SEP particle dispersion in the polymer matrix. For PPgMA composites we see agglomeration of SEP particles and formation of ≈600 nm size clusters. This while in PP + SEP composites these particles are separated from

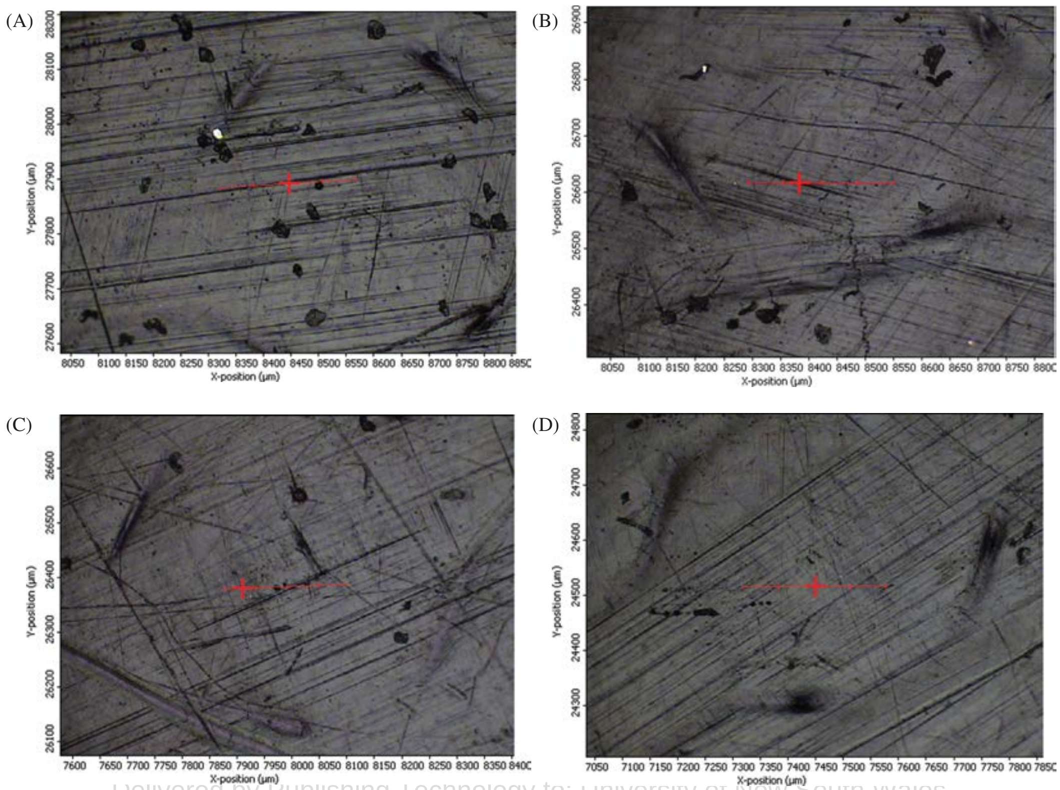

Figure 4. Optical images: PPCNT (A), PPgMA + CNTs (B), PP + CNTOs (C), PPgMA + CNTOs (D).

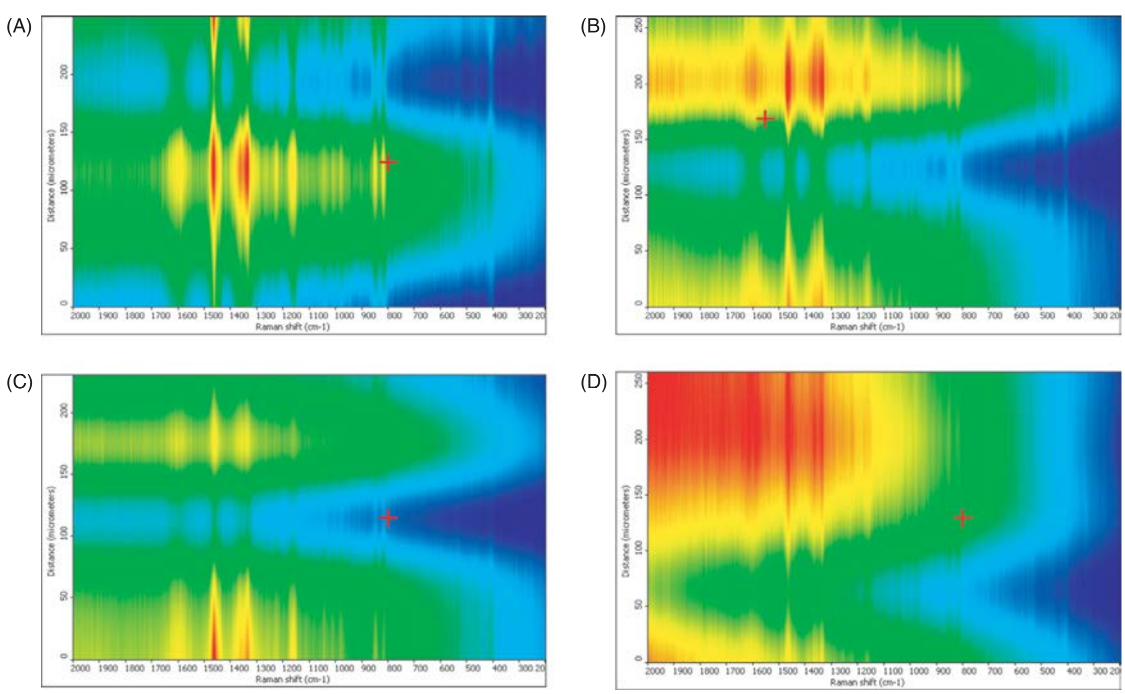

Figure 5. Raman linear mapping spectra: PP + CNTs (A), PPgMA + CNTs (B), PP + CNTOs (C), PPgMA + CNTOs (D).

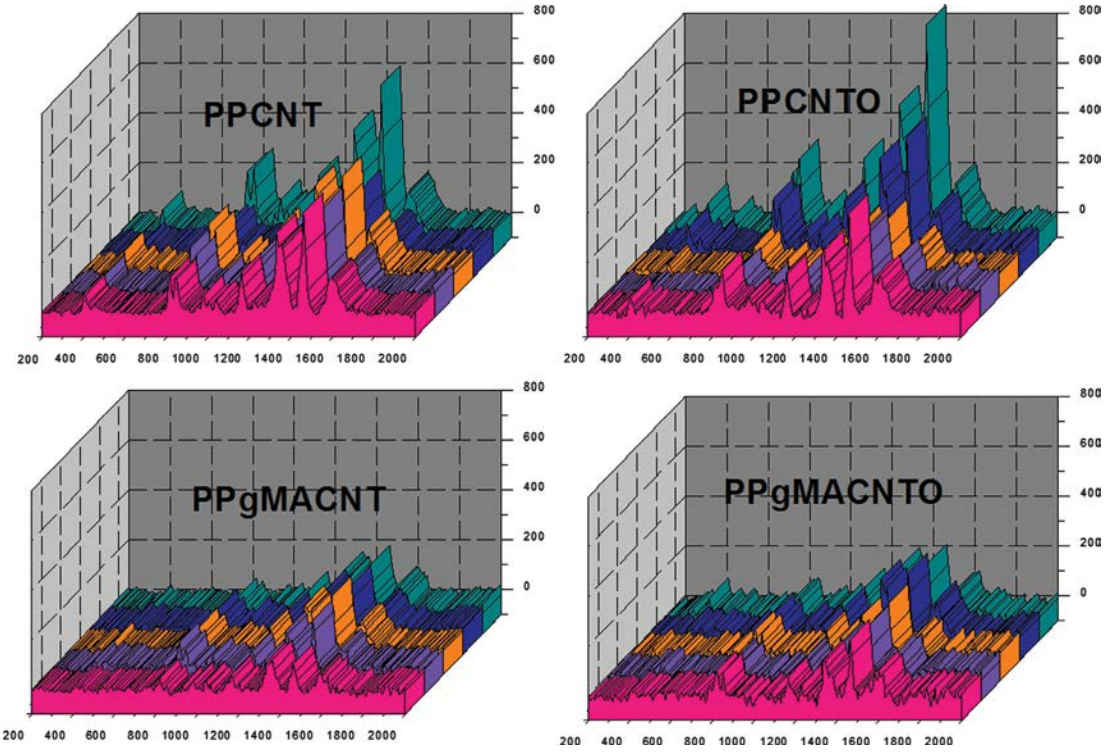

Figure 6. Raman mapping spectra.

each other. The particle agglomerations can be noticed even for the PP sample filled with modified sepiolite but the sizes of the clusters are some twenty times smaller than agglomerates which we found in PpgMA + SEP and/or PpgMA + SEPF. A similar tendency was observed for polymer + Ni composites.[34] In contrast to modified samples, unmodified PP composites show better particle dispersion in all cases. However, there is no adhesion between the particles and the polymer matrix. SEM high magnification images show that inside PP + SEP and PP + SEPF composites, SEP surfaces appear completely 'naked' and almost untouched by PP. In PPgMA both SEP and SEPF particles show good interaction with the polymer. Compared to other samples, PPgMA + SEPF shows improved filler and PP matrix interaction. We can see in Figure 7(D) that nanoparticle surfaces are fully coated and embedded inside PPgMA matrix. Moreover, enhancement of the interfacial interaction is also caused by a decrease in surface energy of the filler through CTABr agent; this leads to improvement of the compatibility of sepiolite with PPgMA through the aliphatic chains of the cethyl group. Overall, introduction of the polar groups inside PP matrix does not help particles dispersion but as a result of increased PP polarity we notice better polymer + filler interactions.

5. SCRATCH RESISTANCE AND HARDNESS

As already noted and eloquently argued by Rabinowicz,[26] wear of materials is significant as a cause of large financial losses to industry because of the need for replacement of parts. Wear is the major cause of materials waste and loss of mechanical performance; any reduction of wear can

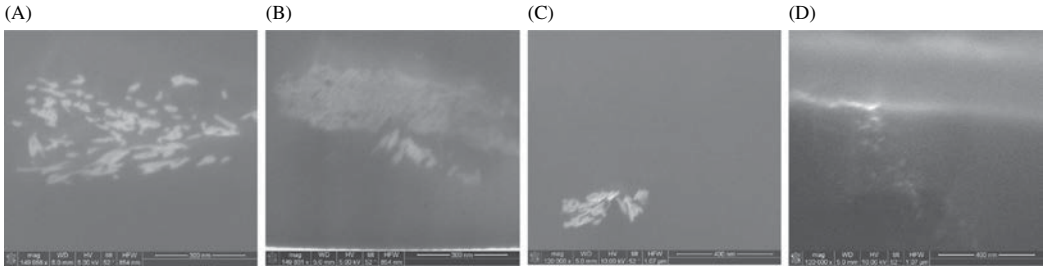

Figure 7. SEM images: PP + SEP (A), PPgMA + SEP (B), PP + SEPF (C), PPgMA + SEPF (D).

result in considerable savings. Further, lowering wear will result in materials and components rejected less frequently and thus in lower contamination of the environment.

We consider scratch resistance first. Three parameters are relevant here: (i) maximum or instantaneous penetration depth R_p; (ii) residual or healing depth R_h (after 2 min); and (iii) percentage viscoelastic recovery φ defined as

$$\varphi = (R_p - R_h)/R_p \cdot 100\% \quad (3)$$

This definition applies to both single scratching, as well as sliding wear determination (SWD), which is performed by multiple scratching along the same groove. In each run, made at a linearly progressive force, we obtain the depth as a function of load, as presented in Figure 8.

Compared to neat PP, PPgMA is less resistant to instantaneous deformation by microscratching. The original penetration depth R_p value of neat PP sample changes from 75 to 275 μm in the 5 to 30 N progressive force range while

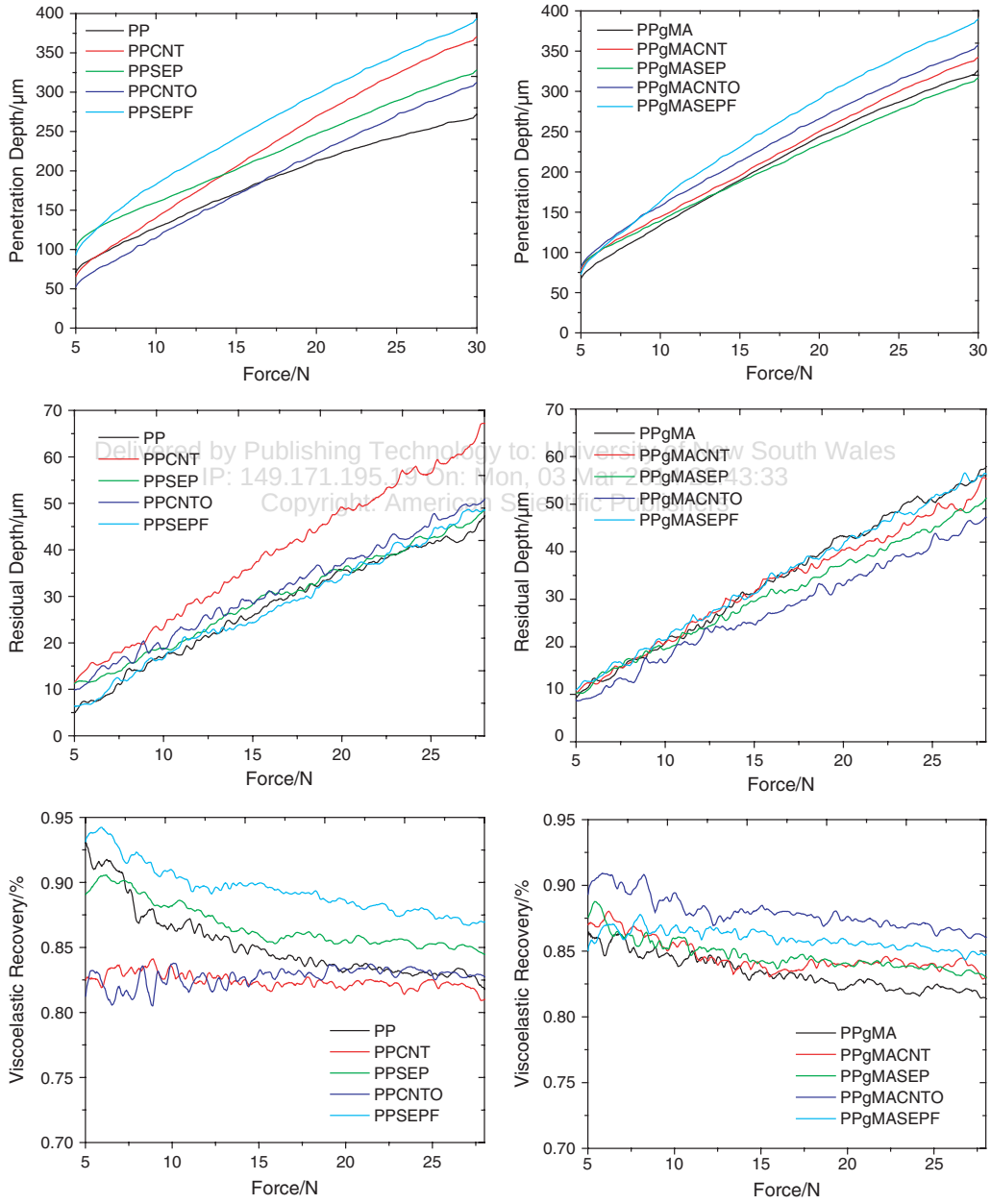

Figure 8. Penetration R_p and residual depth R_h and viscoelastic recovery φ. Left side: PP based materials. Right side: PPgMA based materials. Top: penetration depths; middle: residual depths; bottom; viscoelastic recovery calculated from Eq. (3).

R_p values of the PPgMA material vary in the same load range from 75 to 320 μm. The situation is the same for the residual depth R_h and viscoelastic recovery; namely, the PPgMA sample has relatively larger residual depth and lower percentage of the recovery than PP.

As we see from Figure 8, scratch behavior of the composites changes with load; larger differences between the samples are more evident at high loads. Moreover, most of the PP composites show higher values of R_p than PP; only the PP sample filled with CNTOs behaves similarly to PP and even has lower R_p under 12 to 17 N progressive force.

Residual depth shows materials self recovery (healing) that takes place within 2 min after instantaneous deformation of the material. As we see from Figure 8, PP composites display *slightly* higher values of residual depth; the PP + CNTs sample shows a *much* larger value of R_h. We see that most of PPgMA composites show *shallower* R_h compared to neat PPgMA; the differences between the residual depths of these samples are more pronounced under high applied forces, particularly those above 15 N. For example, under the 20 N load, residual depth of PPgMA is 43 μm while R_h of the PPgMA + CNTOs, PPgMA + SEP and PPgMA + CNTs are 32, 35, 37 μm, respectively. Thus, the 'lack of cooperation' between unmodified PP and its fillers results in the nanocomposites with larger residual depths; by contrast, PPgMA does 'cooperate' with its fillers so that the nanocomposites have smaller R_h values than the neat PPgMA.

Composites prepared with modified sepolite display relatively low scratch resistance. For composites with the PPgMA matrices, the lowest residual depth values are seen for the composites containing modified carbon nanotubes.

Vickers microhardness h_{Vickers} was measured using 3 different loads: 100 N, 300 N and 500 N. The surfaces of the samples have been examined after the indentation

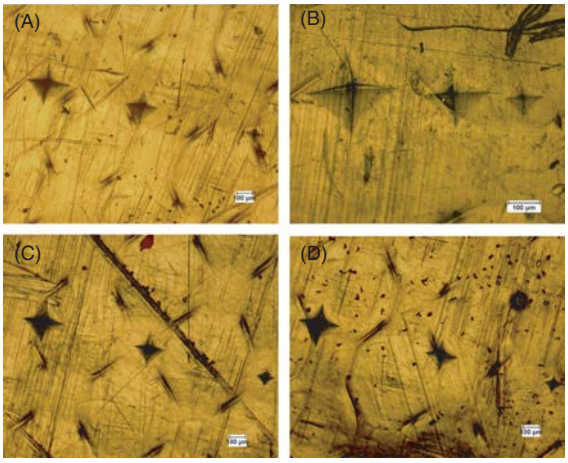

Figure 9. Micrographs of the samples: PP (A), PPgMA (B), PP + CNTs (C) and PPgMA + CNTs (D).

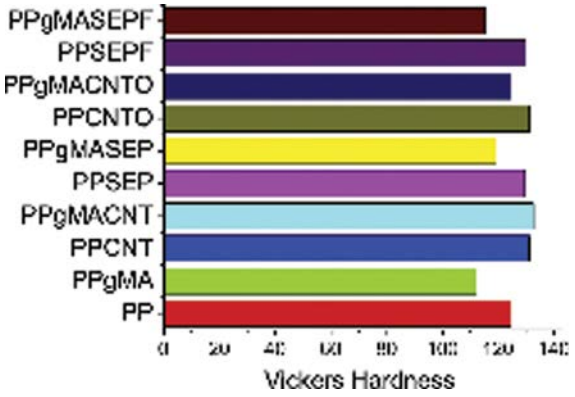

Figure 10. Vickers microhardness.

to observe the differences between the deformed areas. Figure 9 represents the optical micrographs of the indented areas of the samples.

From Figures 9(A) and (B), we see clear differences between indented areas on the PP and PPgMA surfaces. The diagonals of the deformed areas of the PP and PPgMA samples after 500 N applied load are ≈100 μm and 200 μm, respectively. They are equivalent to 113 and 125 hardness values. From Figures 9(C) and (D) we do not see appreciable between indented areas for CNTs composites in PP matrix or PPgMA matrix; the diagonal for both samples are 256 μm after 500 N applied load. Apparently, CNTs weaken the PP matrix as far as point indentation is concerned but they weaken the PPgMA matrix less.

The hardness values are presented in Figure 10. As expected, PPgMA has lower hardness than unmodified PP. The same applies to most nanocomposites, namely containing SEP, SEPF and CNTOs. The only exception is the case of CNTs where the composite based on the PP matrix has almost the same value of hardness as than based on PPgMA. In fact, the latter system has a slightly higher Vickers hardness. Overall, the hardness of the PPgMA materials increases after loading the matrix with any nanofiller. Functionalization of the fillers has practically negligible effects on the hardness.

When we now compare the hardness values with the residual depths, we find that addition of the fillers to PPgMA lowers that depth, that is improves scratch resistance, while it also increases the hardness.

6. FRICTION AND WEAR

Dynamic sliding friction data were collected using a pin-on-disk tribometer by measuring the friction force by means of the deflection of the elastic arm. Strain gauges bonded on the elastic body of the arm convert it into a force sensor and allow the direct measurement of the friction force.

We employed two counterfaces: WC and 302 stainless steel (SS302). Vickers hardness values of the balls are 1300

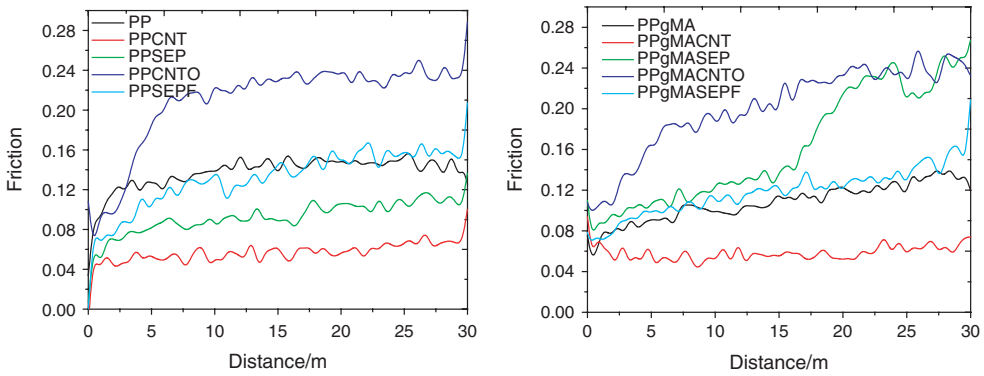

Figure 11. Friction results as a function of distance for the 302 steel ball at 5.0 N.

and 166 for WC and SS302, respectively. We recall that the tests were performed under 5, 10 and 15 N normal force. Figure 11 presents friction diagrams of the nanocomposites recorded applying a 5 N load and a SS302 ball.

Under the 5.0 N load, neat PP and PPgMA show higher friction than PP + CNTs and PPgMA + CNTs, but lower friction than the PP + CNTOs and PPgMA + CNTOs composites. Furthermore, the addition of maleic anhydride *lowers* the friction. Thus, comparing PP with PPgMA, friction goes down from 0.12 to 0.09 after modification.

However, in contrast to PP based composites, almost all PPgMA based *composites show increased friction*. Only the PPgMA + CNTs material is an exception. Increased friction of the PPgMA based composites is related to the particles dispersion. Namely, SEM images of PPgMA composites show formation of the micro clusters due to agglomeration. The size of the clusters is much larger than agglomerated particles found in PP matrix, see again Figure 7. Particles agglomeration decreases material performance because of formation of voids that act as preferential sites for crack initiation and failure.

We recall that PPgMA is a soft material, as seen in lower hardness; during friction testing it undergoes wear easily. PPgMA provides more contacts of the filler to the ball while PP is stiff and cannot be depressed and worn out so easily. The wear results obtained as described in Section 2.2 are shown in Figure 12. Since wear represents separation of the material from the bulk, overall one then has less material plus debris, the wear rates are presented as negative values.

While Figure 12 provides a quick overview, let us consider some numbers. Polypropylene at 15 N has the wear rate $-2.86 \cdot 10^{-5}$ mm^3/Nm. The respective value for PPgMA is much larger, $7.01 \cdot 10^{-4}$ mm^3/Nm. As for nanocomposites, several of them have have higher wear rates than PP. However, also at the 15 N load the wear rate for PP + CNTOs is $-1.92 \cdot 10^{-5}$ mm^3/Nm while for PPgMA + SEP it is $-8.40 \cdot 10^{-6}$ mm^3/Nm. Thus, at least some of our fillers result in significant wear rate lowering.

To get a more comprehensive picture of the situation, consider dynamic friction values at 10.0 N which we display in Figure 13.

First of all, we see in Figure 13 that the friction values at 10 N are closer together than at 5 N; this applies to both PP based and PPgMA based composites. Thus, more differentiation between materials is achieved at lower loads. All PPgMA based materials exhibit higher values of friction compared to PP and its composites. This is expected as we recall that PPgMA is softer than PP. Sepiolite lowers the friction of both PP and PPgMA, significantly so for the former.

PP materials maintain friction in 0.05 to 0.15 range while PPgMA samples keep the friction only short distance and after that the friction curves reach nearly the 0.24 values. After grafting maleic anhydride into PP matrix, the friction climbs dramatically.

As we know, friction always generates heat, thus higher loads could generate greater heat during dry friction tests—which in turn yields higher friction. This is only exacerbated by the presence of MA. Recall that MA is the dehydrated form of maleic acid and we have used it to increase the polarity of PP. When we apply only 5

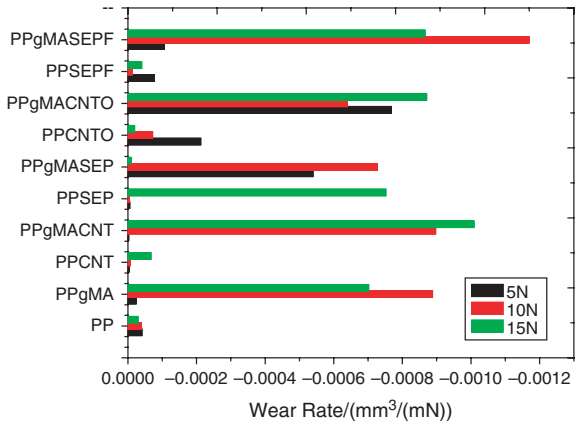

Figure 12. Wear rates for the 302 Steel ball at three load values.

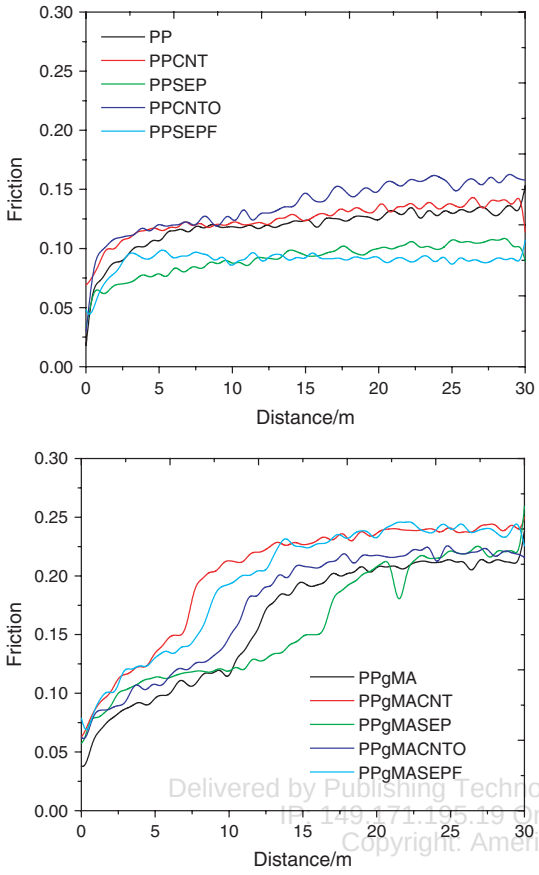

Figure 13. Friction results as a function of distance for the 302 steel ball at 10.0 N.

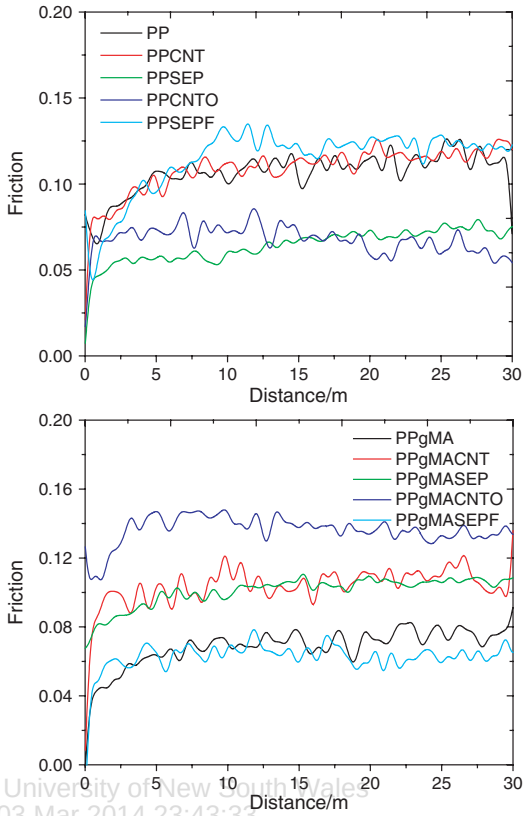

Figure 15. Friction results as a function of distance for the WC ball at 5.0 N.

N loads, then PPgMA exhibits lower friction, even lower than PP due to the lubricating effect of polar groups. However, when we double the load, the situation changes significantly. Higher applied load during friction generates more heat and increases the contact area. Moreover, since PPgMA is a relatively soft material, it is easily depressed by the 10 N of normal force—what also contributes to higher friction. Still further, because of the softness, PPgMA takes more time to reach a steady state than PP, an effect seen also in Figures 14 and 16, less so in Figure 15.

Our explanation is fortified by results for 15 N displayed in Figure 14. At that load, all PPgMA containing samples yield higher friction than those based on PP.

Let us consider now samples containing sepiolite; at a low normal load we observe similar patterns as for CNTs. Namely, sepiolite and CNTs decrease friction of the neat polymers at the 5 N load. However, for sepiolite containing

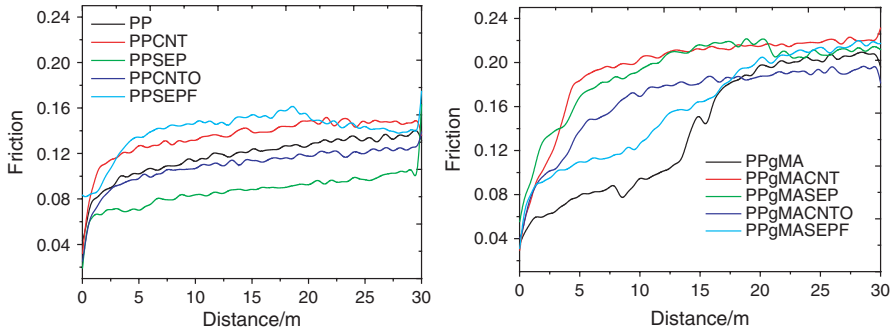

Figure 14. Friction results as a function of distance for the 302 steel ball at 15.0 N.

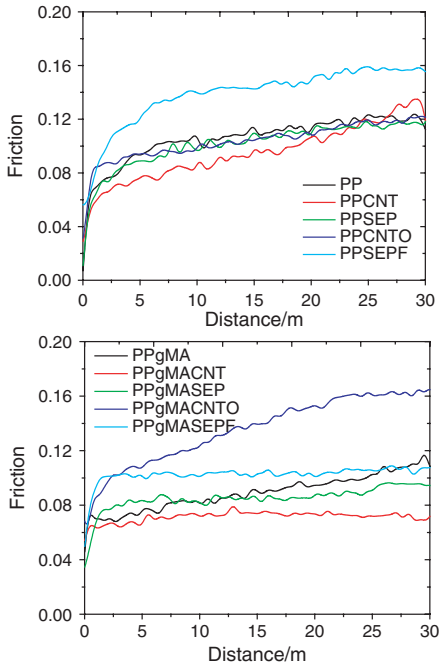

Figure 16. Results as a function of distance for the WC ball at 15.0 N.

samples, there is a difference between the PP based and PPgMA samples. At 10 and 15 N, sepiolite lowers the friction of PP but not of PPgMA. As already noted, the addition of maleic anhydride increases friction values.

We now turn to review the tribological behavior of the samples against WC surfaces. We present results for 5 N in Figure 15 and for 15 N in Figure 16.

Against tungsten carbide, there is a large difference between PP and PPgMA. CNTOs lower the friction of PP, significantly at 5 N and slightly at 15 N. For PPgMA, CNTOs *increase* the friction dramatically, both for 5 N and 15 N.

Given these results, let us compare tribological behavior of our polymers and nanocomposites with respect to 302 stainless steel versus tungsten carbide. At 5 N, CNTs lower the friction of both PP and PPgMA against the steel. At the same load and with WC as the countersurface, CNTs hardly affect the friction of PP while they significantly increase the friction of PPgMA. At 15 N load against the steel, CNTs increase the friction of both PP and PPgMA. At the 15 N load against WC, CNTs affect little the friction of PP while they lower the friction of PPgMA. Thus, in a soft PPgMA matrix against WC which is much harder than steel, CNTs exhibit some lubricating capabilities.

Considering now composites containing sepiolite, we find in these cases similarities between 302 steel and WC as countersurfaces. Sepiolite lowers the friction of PP against both the steel and tungsten surface. As for PPgMA, sepiolite either increases the friction or else hardly affects it (WC at 15 N).

7. CONCLUDING REMARKS

We have studied PP as well as PPgMA, that is polypropylene containing polar groups. As already noted, PP is an important engineering polymer with a wide range of applications.[39] We have applied nanofillers as well as chemically modified nanofillers to affect the compatibility between the matrices and the fillers. We have determined scratch resistance, Vickers hardness, dynamic friction and wear rates. Scratch resistance and the hardness go approximately symbatically; greater scratch resistance is seen for materials with higher hardness. However, there seems to be little to no correlation with scratch resistance and hardness on one side and dynamic friction or wear rates on the other. Experimental determination of all these properties is worthwhile. Clearly, the simple rule that a solid filler should always lower the wear rate of a polymer does not work. Lower wear rates can be achieved with some fillers.

Acknowledgments: We appreciate constructive comments of two reviewers.

References and Notes

1. J. Grebowicz, S.-F. Lau, and B. Wunderlich, *J. Polymer Sci. Symp.* 71, 19 (**1984**).
2. W. Brostow (ed.), Performance of Plastics, Munich-Cincinnati (**2000**).
3. W. X. Chen, F. Li, G. Han, J. B. Xia, L. Y. Wang, J. P. Tu, and Z. D. Xu, *Tribol. Lett.* 15, 275 (**2003**).
4. K. Cowan and Y. Gogotsi, *J. Mater. Ed.* 26, 147 (**2004**).
5. D. S. dos Santos, P. J. G. Goulet, N. P. W. Pieczonka, O. N. Oliveira, and R. F. Aroca, *Langmuir* 20, 10273 (**2004**).
6. D. Hammer and D. Srikantaiah, *J. Mater. Ed.* 26, 245 (**2004**).
7. K. J. Pawlowski, C. P. Barnes, E. D. Boland, G. E. Wnek, and G. L. Bowlin, *J. Mater. Ed.* 26, 195 (**2004**).
8. F. Huguenin, M. Ferreira, V. Zucolotto, F. C. Nart, R. M. Torresi, and O. N. Oliveira, *Chem. Mater.* 16, 2293 (**2004**).
9. M. Meyyappan, *J. Mater. Ed.* 26, 313 (**2004**).
10. A. Nogales, G. Broza, Z. Roslaniec, K. Schulte, I. Sics, B. S. Hsiao, A. Sanz, M. C. Garcia-Gutierrez, D. R. Rueda, C. Domingo, and T. A. Ezquerra, *Macromolecules* 37, 7669 (**2004**).
11. L. C. Klein, *J. Mater. Ed.* 28, 7 (**2006**).
12. D.-B. Shieh, C.-S. Yeh, W.-C. Chang, and Y. Tzeng, *J. Mater. Ed.* 29, 107 (**2007**).
13. R. H. Krämer, M. A. Raza, and U. W. Gedde, *Polym. Degrad. Stab.* 92, 1795 (**2007**).
14. F. P. La Mantia, N. T. Dintcheva, R. Scaffaro, and R. Marino, *Macromol. Mater. Eng.* 293, 83 (**2008**).
15. G. Broza and K. Schulte, *Polym. Eng. Sci.* 48, 2033 (**2008**).
16. L. F. Giraldo, W. Brostow, E. Devaux, B. L. López, and L. D. Pérez, *J. Nanosci. Nanotechnol.* 8, 3176 (**2008**).
17. V. H. Orozco, W. Brostow, W. Chonkaew, and B. L. López, *Macromol. Symp.* 277, 69 (**2009**).
18. W. Brostow, W. Chonkaew, T. Datashvili, and K. P. Menard, *J. Nanosci. Nanotechnol.* 9, 1916 (**2009**).
19. V. H. Orozco, V. Kozlovskaya, E. Kharlampieva, B. L. López, and V. V. Tsukruk, *Polymer* 51, 4127 (**2010**).
20. A. F. Vargas, W. Brostow, H. E. Hagg Lobland, B. López, and O. Olea-Mejia, *J. Nanosci. Nanotechnol.* 9, 6661 (**2009**).
21. A. F. Vargas, V. H. Orozco, F. Rault, S. Giraud, E. Devaux, and B. L. López, *Composites A* 41, 1797 (**2010**).
22. A. Szymczyk, Z. Roslaniec, M. Zenker, M. C. Garcia-Gutierrez, J. J. Hernandez, D. R. Rueda, A. Nogales, and T. A. Ezquerra, *Express Polym. Lett.* 5, 977 (**2011**).

23. A. Kopczynska and G. W. Ehrenstein, *J. Mater. Ed.* 29, 325 **(2007)**.
24. R. C. Desai and R. Kapral, Dynamics of Self-Organized and Self-Assembled Structures, Cambridge University Press, Cambridge, New York **(2009)**.
25. G. H. Michler and F. J. Balta-Calleja, Nano- and Micromechanics of Polymers: Structure Modification and Improvement of Properties, Hanser, Munich, Cincinnati **(2012)**.
26. E. Rabinowicz, Friction and Wear of Materials, Wiley, New York **(1995)**, p. 315.
27. N. K. Myshkin, M. I. Petrokovets, and A. V. Kovalev, *Tribology Internat.* 38, 910 **(2005)**.
28. W. Brostow, J.-L. Deborde, M. Jaklewicz, and P. Olszynski, *J. Mater. Ed.* 25, 119 **(2003)**.
29. W. Brostow, V. Kovacevic, D. Vrsaljko, and J. Whitworth, *J. Mater. Ed.* 32, 273 **(2010)**.
30. E. F. Lucas, B. G. Soares, and E. E. D. C. Monteiro, Caracterização de Polímeros, Determinação de Peso Molecular e Análise Térmica, e-Papers, Rio de Janeiro **(2001)**, p. 366.
31. K. P. Menard, Thermal transitions and their measurement, Performance of Plastics, edited by W. Brostow, Hanser/Gardner Publications, Cincinnati **(2000)**, p. 147.
32. U. W. Gedde, Polymer Physics, Springer-Kluwer, Dordrecht-Boston **(2001)**, p. 301.
33. W. Brostow, B. P. Gorman, and O. Olea-Mejia, *Mater. Lett.* 61, 1333 **(2007)**.
34. W. Brostow, M. Brozynski, T. Datashvili, and O. Olea-Mejía, *Polym. Bull.* 59, 1671 **(2011)**.
35. W.-M. Chiu and Y.-A. Chang, *J. Appl. Polym. Sci.* 107, 1655 **(2008)**.
36. V. Datsyuk, M. Kalyva, K. Papagelis, J. Parthenios, D. Tasis, A. Siokou, I. Kallitsis, and C. Galiotis, *Carbon* 46, 833 **(2008)**.
37. G. Sandí, R. E. Winans, S. Seifert, and K. A. Carrado, *Chem. Mater.* 14, 739 **(2002)**.
38. M. Alkan, G. Tekin, and H. Namli, *Microporous Mesoporous Mater.* 84, 75 **(2005)**.
39. J. Karger-Kocsis, Polypropylene—An A–Z Reference, Chapman and Hall, London **(1999)**.

Received: 2 January 2013. Accepted: 20 April 2013.